WIND ENERGY
Wind Energ. 2009; **12**:33–49
Published online 11 June 2008 in Wiley Interscience
(www.interscience.wiley.com) DOI: 10.1002/we.281

Control Strategy of a Wind Turbine Drive by an Integrated Model

M. Andriollo, M. De Bortoli, G. Martinelli, A. Morini and A. Tortella*, Department of Electrical Engineering, University of Padova, Via Gradenigo 6/A, 35131 Padova, Italy

Key words:
permanent magnet direct-drive generator; circuit model; sensorless control strategy; control robustness

In this paper, an integrated equivalent circuit is defined to analyse the operation of a wind generator–rectifier system connected to a DC link, with the electric machine consisting of a surface-mounted permanent magnet synchronous generator (SPMG) directly coupled to the wind turbine. Such circuit is defined by integrating the models related to the electromechanical equations implemented into a Simulink® code, where the SPMG parameters are derived by the elaboration of sequences of magnetostatic FEM analyses. The integrated equivalent circuit can be very useful to examine the wind generator dynamics because of wind speed variations, and to analyse the influence of the electromechanical parameters on the energy output in order to identify the appropriate control strategies involving the regulation of the rotor speed, the DC link current and the blade pitch angle. In particular, a sensorless algorithm is implemented to estimate the main mechanical quantities (output torque and rotor speed) and to determine the wind speed by means of only electrical measurements. The comparison with an anemometer-based solution shows that similar performances can be achieved in different operating conditions. The control strategies set up by the circuit model are verified on a 20 kW-rated SPMG with outer rotor, comparing the sensor and sensorless approaches in terms of capability of energy production, dynamic promptness and sensitivity to parameter disturbances, also with wind turbulence. Copyright © 2008 John Wiley & Sons, Ltd.

Received 28 January 2008; Revised 30 April 2008; Accepted 10 May 2008

Introduction

In the field of renewable energy systems for distributed generation, the increasing demand of low-rated wind generators calls for the development of more efficient and low-cost systems by the integration of the design choices and of the control strategy governing the electromechanical behaviour. The use of enhanced simulation tools is therefore essential to predict the transient and steady-state performances, as well as to tune the control algorithm in order to maximize the output power, bearing in mind both the mechanical and the electromagnetic constraints.

In this paper, an integrated equivalent circuit is defined to analyse the operation of a wind generator–rectifier system, with the electric machine consisting of a surface-mounted permanent magnet synchronous generator (SPMG) directly coupled to the wind turbine. The configuration is particularly convenient, thanks to the good efficiency (absence of the gearbox and the rotor winding supply), to the installation simplicity (drive-train

* Correspondence to: A. Tortella, Department of Electrical Engineering, University of Padova, via Gradenigo 6/A, 35131 Padova, Italy.
E-mail: tortella@die.unipd.it
Sponsor: Italian National Ministry of University and Scientific Research (MiUR), PRIN 2005, Title: 'Design and Optimization of Generators for the Production of Wind Electrical Energy'.

simplification, reduced number of components, reduced weight and volume of the nacelle especially for low-power wind generators), to the wide control range of the electromagnetic torque by varying the DC link voltage and to the limited costs (reduced maintenance and absence of AC–DC bidirectional converters). A pitch angle regulation is also considered to improve the turbine utilization at high wind speed; this solution makes the turbine manufacturing and management more complex, but improves the power output at high wind speed without exceeding the design ratings.

The equivalent circuit is defined by integrating the models related to the mechanical and electrical equations. First, the torque balance is represented by means of an electrical analogy, with torques and angular speeds replaced by electrical currents and voltages, respectively. Then, the electrical behaviour is described by using a simplified circuit representing the SPMG–rectifier–DC load system, implemented into a Simulink code. The SPMG parameters are derived by the elaboration of sequences of magnetostatic FEM analyses. The simplified circuit takes into account the e.m.f. full harmonic content, the magnetic saturation because of the permanent magnets and the non-linear voltage drop caused by the rectifier commutation.

The integrated equivalent circuit can be very useful to examine the wind generator dynamics caused by wind speed variations, and to analyse the influence of the electromechanical parameters on the energy output in order to identify the appropriate control strategies. In particular, the circuit model makes also possible the implementation of a sensorless algorithm to estimate the main mechanical quantities (output torque and angular speed), and to determine the wind speed by means of only electrical measurements. The comparison with an anemometer-based solution shows that similar performances can be achieved in different operating conditions. Moreover, a strategy for the regulation of the DC link current and of the blade pitch angle is developed to optimize the system performances in an extended range of the wind speed.

As an example of application, the proposed control strategies are verified on a 20 kW-rated SPMG with outer rotor, and the sensor and sensorless approaches are compared in terms of capability of energy production, response time to wind speed variations and sensitivity to parameter disturbances, also with wind turbulence.

Equivalent Circuit

The instantaneous power balance at the turbine shaft is:

$$P_t = P_{em} + P_m + J\frac{d\Omega}{dt}\cdot\Omega \tag{1}$$

where Ω is the angular speed, P_t is the turbine power, P_{em} SPMG is the electromagnetic power, P_m is the mechanical loss and J is the total momentum of inertia. The power P_t is proportional to the cubic of the wind speed v according to the well-known relation:[1]

$$P_t = k_c C_p(\lambda,\beta)\, v^3, \quad k_c = \pi/2R_t^2\rho \tag{2}$$

where R_t is the turbine radius and ρ is the air density. The power coefficient C_p is a function of both the tip-speed ratio $\lambda = \Omega R_t/v$ and the blade pitch angle β; it can be formulated by an analytical expression, once the fluid dynamic model is known or, alternatively, by the interpolation of experimental data.

The turbine torque T derives from equation (2) according to:

$$T = P_t/\Omega = k_T C_p(\lambda,\beta)/\lambda\cdot v^2, \quad k_T = k_c\cdot R_t \tag{3}$$

The losses P_m, sum of the friction and windage losses, can be expressed as follows:[2]

$$P_m = \left(k_{ft} + k_w\cdot\Omega^2\right)\cdot\Omega, \quad k_{fr} = t_{fr}T^*, \quad k_w = t_w\left(\Omega/\Omega^*\right)^2 T^* \tag{4}$$

where Ω^*, T^* are the turbine rated speed and torque, respectively, and t_{fr}, t_w are the per unit friction and windage torques at the rated speed, respectively. The corresponding torque T_m is therefore given by:

$$T_m = P_m/\Omega = k_m(\Omega)\cdot\Omega, \quad k_m = k_{fr}/\Omega + k_m\Omega \tag{5}$$

DOI: 10.1002/we

The coefficient k_m takes into account the non-linear dependence of T_m on the angular speed Ω.

Bearing in mind equations (3) and (5), the relation $T_{em} = P_{em}/\Omega$ and using the analogy between mechanical and electrical quantities, the balance [equation (1)] can be associated to the equivalent electric circuit of Figure 1;[3] the solution of this non-linear circuit makes possible the analysis of the dynamic behaviour of the wind turbine, once T_{em} is known.

In order to define the equivalent circuit related to the electric behaviour, the SPMG model is developed: the phase e.m.f.s $e_{PM,j}$ ($j = 1, 2, 3$) because of the magnets as well as the self and mutual inductances L and M as functions of the rotor position are calculated by interpolating the results of 2D non-linear magnetostatic FEM analyses at no load.[4] By assuming an isotropic magnetic configuration and no neutral wire, the electric model is implemented into a Simulink code (Figure 2(a)), including the phase resistance R and the equivalent constant phase inductance L–M: this makes possible the determination of the instantaneous voltages and currents, as well as the output power as functions of the rotor speed Ω and of the load current i_{dc}, taking into account the commutation effects.

In particular, by assuming a large DC link inductive filter ($i_{dc} = I_{dc} = \text{const.}$), the load voltage U_{dc} is interpolated as a function of I_{dc} and Ω by means of the polynomial fitting:

$$U_{dc}(\Omega, I_{dc}) = \sum_{h=0}^{m}\sum_{k=1}^{n} a_{h,k}\Omega^k I_{dc}^h \tag{6}$$

where $a_{h,k}$ are the coefficients of the $m \times n$ order polynomial. It is worth to point out that $h = 0$ corresponds to the no-load rectified voltage U_{d0}; since generally $a_{0,k} << a_{0,1}$ for $k > 1$, it is:

$$U_{d0} \approx a_{0,1} \cdot \Omega = k_v \cdot \Omega \tag{7}$$

The application of equation (6) allows to define an equivalent circuit related to the DC link supply and to evaluate the SPMG–rectifier output characteristic. To such purpose, the voltage equation can be written as:

$$U_{d0} = U_{dc} + (R_{dc} + 2R) \cdot I_{dc} \tag{8}$$

from which the equivalent non-linear commutation resistance R_{dc} can be found as:

$$R_{dc}(\Omega, I_{dc}) = \frac{U_{d0} - U_{dc}}{I_{dc}} - 2R \approx \frac{k_v \cdot \Omega - U_{dc}(\Omega, I_{dc}) - 2RI_{dc}}{I_{dc}} \tag{9}$$

The circuit representation of equation (8) is shown in Figure 2(b), where the following parameters are also included:

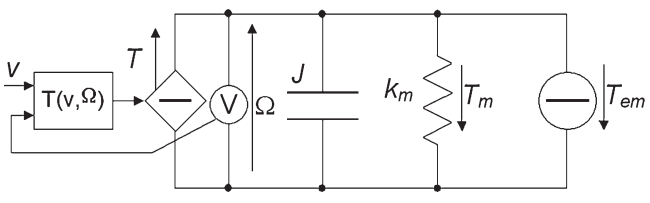

Figure 1. Equivalent circuit describing the system mechanical behaviour

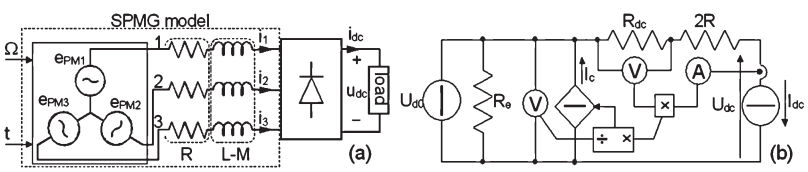

Figure 2. Equivalent electrical circuits: (a) surface-mounted permanent magnet synchronous generator (SPMG)–rectifier model; (b) DC link supply system

DOI: 10.1002/we

- A controlled current source I_c, compensating the fictitious active power associated to the commutation resistance:

$$I_c = \frac{R_{dc} I_{dc}}{U_{d0}} \cdot I_{dc} \tag{10}$$

- An equivalent resistance R_e, associated to the no-load electromagnetic losses (iron losses P_{fe} and permanent magnet losses P_{PM}), as the contribution caused by the armature reaction is generally negligible in the SPMGs; the value of R_e is expressed as:

$$R_e(\Omega) = \frac{U_{d0}^2}{P_{fe} + P_{PM}} \tag{11}$$

The determination of both iron and PM losses is carried out by elaborating the results of a sequence of FEM magnetostatic analyses, according to the numerical procedure described in Andriollo *et al*.[4] The losses at the generic operating speed Ω can be obtained by the corresponding values at the rated speed Ω^* according to:

$$\begin{aligned} P_{fe} &= p_h^* \cdot \frac{\Omega}{\Omega^*} + p_{ec}^* \cdot \left(\frac{\Omega}{\Omega^*}\right)^2 + p_{ex}^* \cdot \left(\frac{\Omega}{\Omega^*}\right)^{3/2} \\ P_{PM} &= p_{ec,PM}^* \cdot \left(\frac{\Omega}{\Omega^*}\right)^2 \end{aligned} \tag{12}$$

where p^*_h, p^*_{ec}, p^*_{ex} are the total hysteresis, eddy current and excess losses in the laminated cores, respectively, and $p^*_{ec,PM}$ are the PM eddy current losses at Ω^*.

The equivalent circuits of Figures 1 and 2 can be integrated into only one circuit according to equation (7), which formally corresponds to the relation between the primary and secondary voltages of an ideal transformer with transformation ratio k_v and primary voltage Ω. The resulting integrated circuit of Figure 3 can be useful in the formulation of the control strategy, because the evolution of the electrical quantities describes univocally the system dynamic behaviour, once the wind speed is given. The equivalent resistance R_0 represents both the electromagnetic and mechanical losses, and it is formally related to the total no-load losses $P_0 = P_m + P_{fe} + P_{PM}$. With reference to equations (5) and (11), R_0 is given by:

$$R_0(\Omega) = \frac{k_v^2 k_m R_e}{k_v^2 k_m + R_e} \tag{13}$$

Control Strategy

The control strategy aims at the maximization of the wind generator output power at any wind speed in the operating range, consistently with the electrical, thermal and mechanical design constraints. To such purpose, the control quantities (the load current I_{dc} and the pitch angle β) must follow a suitable variation rule, fulfilling both the power balance [equation (1)] and the mentioned constraints.

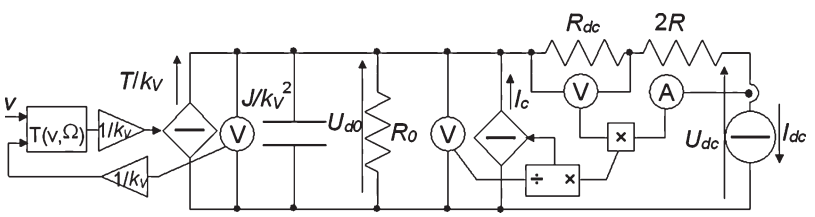

Figure 3. Integrated equivalent circuit related to the wind turbine–surface-mounted permanent magnet synchronous generator–rectifier system

DOI: 10.1002/we

Let $v_{cut,in}$, v^*, $v_{cut,off}$ the cut-in, rated and cut-off wind speed values, respectively; Ω_M the maximum rotor speed according to the mechanical constraints; and v_M the corresponding wind speed; three different strategies are adopted:

- In the range $v_{cut,in} \le v \le v^*$, the operating point corresponds to the tip-speed ratio value λ_M maximizing the power coefficient with $\beta = 0^\circ$, i.e., $C_p[\lambda_M(0),0] = C_{pM,0}$; the angular speed varies proportionally with the wind speed according to the relation:

$$\Omega = \lambda_M(0) \cdot v / R_t \tag{14}$$

- In the range $v^* \le v \le v_M$, the load current is maintained at the rated value $I_{dc}{}^*$, and the pitch angle is varied to control the rotor speed increase as a function of the wind speed; since $\Omega > \Omega^*$, a slight voltage overrating of the power converter is required;
- In the range $v_M \le v \le v_{cut,off}$, the load current is still maintained at $I_{dc}{}^*$ and the pitch angle is regulated to keep the rotor speed at Ω_M, resulting in constant output power as well.

On the basis of the described strategies, the reference values $I_{dc,r}(v)$ of the DC current and $\beta_r(v)$ of the pitch angle can be defined as functions of the wind speed, once the electromechanical characteristics of the wind generator–load system are known.

In the usual control strategies, $v^* = v_M$ is assumed, i.e., the generator-rated power corresponds to the power supplied by the turbine at $\Omega = \Omega_M$ with $\beta = 0^\circ$;[5] nevertheless such approach may lead to an excessive generator sizing, especially when the wind generator mainly operates in the low- and medium-speed range. On the contrary, the proposed technique aims to limit the generator current rating which corresponds to a rated wind speed $v^* < v_M$, allowing at the same time to exploit higher wind speed values.

With reference to the operating conditions (first), several techniques are proposed in the applications so that the turbine operates at the maximum power (maximum power point tracking or MPPT),[1,6,7]

In the paper, the operation at $\lambda = \lambda_M$ is attained by the control of the current I_{dc} to adjust the electromagnetic torque in order to match the wind speed variations. On the basis of the power balance, it is for the reference values:

$$2RI_{dc,r}^2 + U_{dc}(\Omega_r, I_{dc,r}) \cdot I_{dc,r} = 2RI_{dc,r}^2 + P_{dc,r} = P_t(v) - P_0(\Omega_r) \tag{15}$$

where Ω_r is given by equation (14) and $P_{dc,r} = U_{dc,r}(\Omega_r, I_{dc,r}) \cdot I_{dc,r}$ is the reference value of the power delivered to the DC load. The solutions of equation (15) in the $I_{dc,r}$ unknown are interpolated for different values of v by means of a polynomial function according to:

$$I_{dc,r}(v) = \sum_{k=0}^{n} b_k v^k \tag{16}$$

In order to quickly attain the rotor speed determined by the MPPT strategy and to reduce the mechanical stress in the starting phase, an implementation subdivided into two operating steps is proposed in the paper: at first, the turbine speed increases without load up to $\Omega = k_\Omega \Omega_r$ ($k_\Omega < 1$), then the reference value of the current is applied with a ramp time profile. Some preliminary simulations have, however, pointed out that oscillations of the main mechanical quantities are still possible, because of disturbances superimposed on the value of the wind speed, both when such value is directly measured and when it is estimated in sensorless applications; accordingly, a low-pass filter has been added, in order to get sufficiently regular current profile.

If the wind speed is over the rated value (second operating conditions), the operation at constant power with $\Omega = \Omega^*$ and $I_{dc} = I_{dc}{}^*$ is generally proposed; alternatively, the variation of the reference values is arranged in the paper by using the power balance with $I_{dc} = I_{dc}{}^*$, i.e.,

$$k_P C_P(\Omega_r R_t / v, \beta_r)\, v^3 = P_0(\Omega_r) + 2RI_{dc}^{*2} + P_{dc}^* \tag{17}$$

once a predefined voltage overload is allowed. In order to define the optimum variation law for β_r, a possible approach is to use equation (17) to determine the speed v as a function of β and Ω, once the $C_P(\lambda,\beta)$

DOI: 10.1002/we

characteristic is known. In particular, by constructing the v iso-value curves, the β values maximizing the rotor speed and then the power at the generator shaft can be determined: by analytically interpolating the obtained data, the function $\beta_r(v)$ to be used in these operating conditions is found.

When the maximum allowable rotor speed is reached (third operating conditions), the $\beta_r(v)$ characteristic is found by numerically resolving equation (17) with $\Omega_r = \Omega_M$.

Implementation of the Control System Algorithm

The implementation of the described control strategy has been carried out with reference to both applications with wind and rotor speed sensors and sensorless applications.The procedure is the same for both the approaches and can be summarized as follows (Figure 4):

- The wind speed v (estimated or as anemometer signal) is used to preliminary generate the reference values of the rotor speed Ω_r, the current $I_{dc,r0}$ and the pitch angle β_r.
- Given the rotor speed (estimated or as encoder signal), the speed error $\Delta\Omega$ is calculated and used to adjust the values of v and $I_{dc,r0}$ by means of the variations Δv and $\Delta I_{dc,r}$ produced by suitable regulation algorithms: the adjusted speed value v' is used to generate the reference values Ω_r, $I_{dc,r0}$, β_r, while the adjusted value $I_{dc,r}$ is in turn used to control the load converter.
- The reference value of the blade pitch angle is sent to the control circuit of the actuator system; the circuit generates the desired β value, in accordance with prearranged dynamics which takes into account of both the stress constraints and the system promptness.

In the sensorless configuration, the main mechanical quantities are determined only by electrical measurements, utilizing the mechanical model of the turbine and the circuital model of the generator and load. The aim is to get a reliable estimation of the wind speed to set up the reference values $I_{dc,r}$, Ω_r and β_r on the basis of the previously described control strategies.

Estimation of the Turbine Angular Speed and Torque

By solving equation (6) in Ω for different values of U_{dc} and I_{dc}, the function $\Omega(U_{dc},I_{dc})$ is defined, making possible to evaluate the speed as a function of the voltage and current measurements.

As far as the turbine torque, the torque balance equation is considered, expressed in terms of L-transforms:

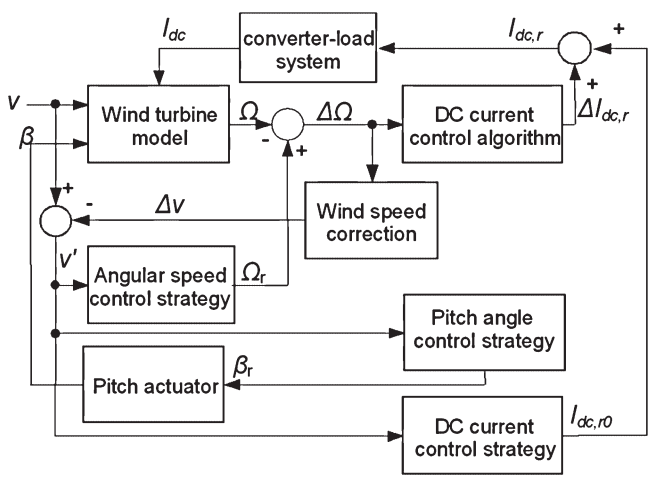

Figure 4. Block diagram of the control algorithm

DOI: 10.1002/we

$$T = T_{em} + T_m + Js\Omega = T_0 + T_1 + Js\Omega \tag{18}$$

where T_0 is the no-load resistant torque, and T_1 is its increase in load conditions. With reference to the circuit of Figure 3, it is:

$$\begin{aligned} T_0 &= \frac{U_{d0}^2 / R_0}{\Omega} \\ T_1 &= \frac{P_{dc} + 2RI_{dc}^2}{\Omega} \end{aligned} \tag{19}$$

The resistance R_0 is found by means of equation (13), once the speed $\Omega(U_{dc},I_{dc})$ is known. Therefore, the relations [equation (19)] define two functions which can be determined on the basis of only electrical quantities. In order to avoid numerical problems produced by the numerical discrete process in the simulation or by the noise physically present in the application, the term corresponding to the inertial torque $Js\Omega$ is replaced by the following transfer function:

$$\frac{Js\Omega}{(1+\tau_m s)^2} \tag{20}$$

The time constant $\tau_m = 1/f_m$ is chosen on the basis of the bandwidth frequency f_m, fixed in advance according to the system physical characteristics and to the accuracy requirements.

Estimation of the Wind Speed

The absence of the anemometer can be very convenient, because it implies both the reduction of the cost (removal of the sensor and of the components for the signal conditioning and transmission) and the elimination of the problems related to the sensor positioning. The developed algorithm aims to find analytically the value of the tip-speed ratio as a function of T and Ω. By substituting $v = \Omega R_t/\lambda$, the torque equation (3) becomes:

$$T = k_{t1} \frac{C_p(\lambda, \beta)}{\lambda^3} \Omega^2, \quad k_{t1} = k_t R_t^2 \tag{21}$$

Rearranging such equation and using the turbine torque and speed values T and Ω (directly measured or estimated as previously described), the following equation is obtained with λ as unknown:

$$\frac{C_p(\lambda, \beta)}{\lambda^3} = F, \quad F = \frac{T}{k_{t1}\Omega^2} \tag{22}$$

The solution of equation (22), as the parameters F and β vary, makes possible, in principle, the definition of the function $\lambda = \lambda(F,\beta)$ to determine the tip-speed ratio. Actually, the values of F are obtained for a prearranged set of values $\{\lambda,\beta\}$ and, successively, $\lambda(F,\beta)$ is defined through an inverse interpolation. An estimation of the wind speed as $v' = \Omega R_t/\lambda(F,\beta)$ can be therefore obtained. With reference to the analytical formulation of $\lambda(F,\beta)$, problems related to its non-biuniqueness with F may be present. Practically, these problems are solved by considering, in the steady-state running, only the region of the characteristic which corresponds to stable operation. As the turbine operates in the other regions only in particular transient conditions (hence, speed tracking accuracy is not required), the actual characteristic is 'corrected' in order to fulfil the $\lambda \leftrightarrow F$ biuniqueness; in this way, problems in the control implementation are avoided, ensuring anyway the outlet of the operating point from the unstable region.

Definition of the Speed Feedback Control Loop

The control system must be designed to drive the turbine at the optimum steady-state working point, avoiding the unstable zone of the C_p characteristic ($\lambda < \lambda_M$); further, it must be robust as far the influence of parametric

DOI: 10.1002/we

variations as well as of measurement inaccuracies (e.g. because of the air density variation or to the anemometer signal). To such purpose, two correction circuits have been set up, as previously outlined (Figure 4); they act, respectively, on the current reference $I_{dc,r}$ and on the wind speed value v (estimated or provided by the anemometer). The complete control procedure for both the sensorless and the sensor-provided configurations is outlined in Figure 5: in particular, the blocks related to the estimation of the mechanical quantities for the sensorless configuration and the mentioned correction blocks are pointed out.

As far as the determination of $\Delta I_{dc,r}$, the relation between the angular speed variation $\Delta\Omega$ and the load current variation ΔI_{dc} has been expressed through a simplified transfer function, based on the circuit representation of Figure 3; according to such relation, the parameters of the transfer function R_i of the regulator (Figure 5) are defined in the following.

By linearizing the dynamical behaviour of the system around a steady-state working point, defined by the values Ω_r and T_r and obtained according to the described strategy, the torque balance equation may be rewritten as:

$$\frac{\Delta T}{k_v} = \frac{J}{k_v}\frac{d\Delta\Omega}{dt} + \frac{k_v}{R_0}\Delta\Omega - \Delta I_c + \Delta I_{dc} \tag{23}$$

The relation corresponds to the balance for the current variations in the circuit of Figure 3. As far as the turbine torque variation, it is:

$$\frac{dT}{d\Omega} = \frac{\partial T}{\partial\lambda}\frac{\partial\lambda}{\partial\Omega} + \frac{\partial T}{\partial\Omega} = -\frac{T}{\Omega} \Rightarrow \frac{\Delta T}{\Delta\Omega} = -\frac{T_r}{\Omega_r} \tag{24}$$

The variation ΔI_c, obtained by the differentiation of equation (10), consists of higher-order infinitesimals and then is not considered. By rewriting equation (23) in terms of L-transforms and by resolving with respect to $\Delta\Omega$, it results:

$$\Delta\Omega(s) = -\frac{1}{k_v/R_0 + T_r/(k_v\Omega_r) + J/k_v s}\Delta I_{dc}(s) = -\frac{G_i}{1+s\tau_i}\Delta I_{dc}(s) \tag{25}$$

where G_i is the static gain and τ_i is the time constant, given respectively by:

$$G_i(\Omega_r) = \frac{1}{k_v/R_0 + T_r/(k_v\Omega_r)}, \quad \tau_i(\Omega_r) = \frac{1}{k_v^2/R_0 + T_r/\Omega_r} \tag{26}$$

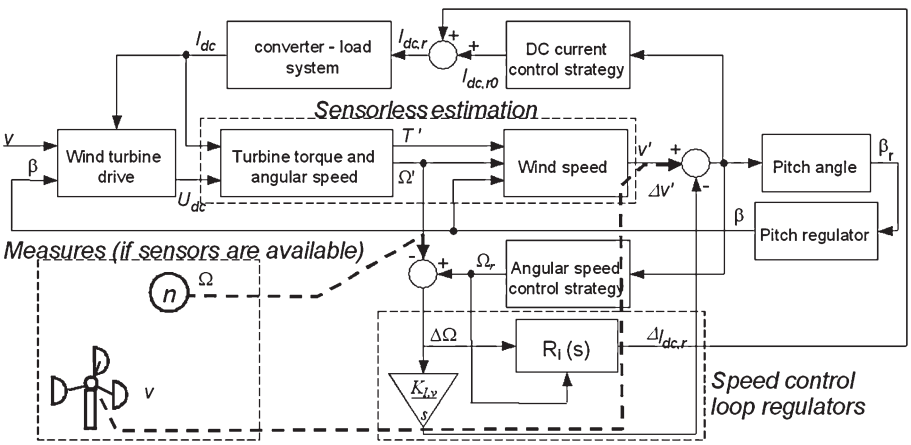

Figure 5. Complete control procedure for the sensorless and the sensor–provided configuration (T', Ω', v': estimated values; dashed lines represent the sensor signals, if available)

DOI: 10.1002/we

The wind generator is therefore reproduced by a first-order system, with gain dependent on the rotor speed. By means of equation (26), G_i can be interpolated with two polynomial functions of Ω_r according to:

$$\begin{aligned} G_i(\Omega_r) &= \sum_{k=0}^{4} c'_k \cdot \Omega_r^k \quad \Omega_r \le \Omega^* \\ G_i(\Omega_r) &= \sum_{k=0}^{2} c''_k \cdot \Omega_r^k \quad \Omega^* \le \Omega_r \le \Omega_M \end{aligned} \tag{27}$$

The parameters related to the regulator transfer function R_i are chosen on the basis of equation (27) for the sensor-provided and sensorless configurations.

In the case of anemometer-provided system, it is necessary to use a PI controller to avoid errors in the steady-state conditions and to compensate possible parametric variations, while in the case of sensorless system, a pure proportional action is adequate to ensure the accuracy and stability requirements. The utilized expressions are therefore:

$$R_i(s) = \begin{cases} K_{P,i} + K_{I,i}/s = (1 + s\tau_R)/(sG_i\tau_R) & \text{with anemometer} \\ K_{P,i} & \text{sensorless} \end{cases} \tag{28}$$

with $K_{P,I} = 1/G_i(\Omega_r)$, $K_{I,I} = K_{P,i}/\tau_R$ and time constant τ_R, chosen close to $\tau_i(\Omega^*)$.

The term $\Delta v'$, compensating the angular speed error $\Delta\Omega$, affects the generation of both the current reference value $I_{dc,r0}$ and the pitch angle reference value β_r, in order to: (i) correct, at steady state, the effects of the measurement errors introduced by the anemometer (device inherent errors, errors caused by the speed non-uniformity in the air stream); (ii) compensate the parametric variations, such as the air density, in both the sensor-provided and sensorless systems; the latter are anyway inherently less affected by such variations; and (iii) improve the dynamical response of the system and reduce the dynamical stresses at the same time.

The correction $\Delta v'$ is generated by modulating the angular speed error $\Delta\Omega$ (Figure 5) through an integral action which removes the steady-state error: the corresponding gain $K_{I,v}$ is fixed to fulfil the requirements on both the system promptness and the limitation of the power fluctuations. The results of the simulations have confirmed that the correction $\Delta v'$ makes possible, even with anemometer errors, to obtain performances very close to the ones of an error-free anemometer system.

Reduction of the Blade Pitch Actuator Operation

The adopted strategy for the control of the pitch angle β aims to simplify the system configuration and to limit the actuator operation with high-rate variations of the reference β_r. The rate of β variation is imposed to be 0 or $\pm\omega_\beta$, according to the value 0 or ±1 of the driving signal d at the input of the block $R_\beta(s)$ (Figure 6(a)); such signal is the sum of the signals from two hysteresis bands (HB_1 and HB_2) displaced by $\varepsilon_1 - \varepsilon_2$ (Figure 6(b)), whose outputs are equal to $\{0,1\}$ and $\{-1,0\}$, respectively. The choice of the thresholds ε_1 (switch-on point)

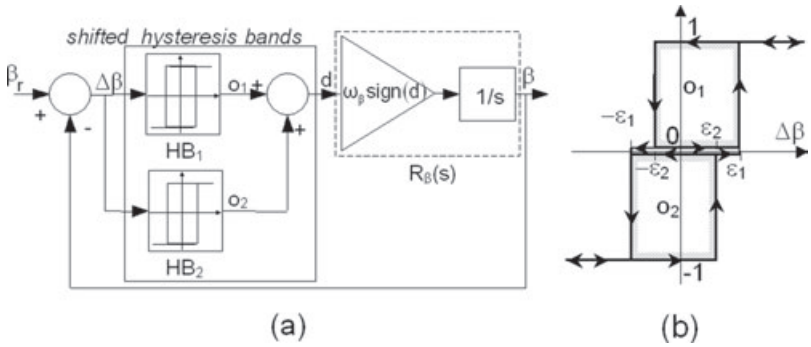

Figure 6. Procedure of the pitch angle control: general scheme (a) and dual hysteresis band (b)

DOI: 10.1002/we

and ε_2 (switch-off point) affects both the start–stop frequency of the pitch actuator and the accuracy and the promptness in tracking β_r; after all, such choice affects the dynamical stress on the turbine in transient conditions (overspeed) and the energy efficiency.

Example of Application

The proposed control procedure has been applied to a 20 kW turbine–SPMG–rectifier system. The four-pole cross section of the SPMG is shown in Figure 7. The machine is provided with 32 NdFeB magnets (pole pairs $p = 16$) with axial length $l_m = 200$ mm. The values of the electrical parameters are $k_v = 46.12$ Vs, $R = 0.56\ \Omega$ and $L–M = 18.97$ mH; the rated current is $I_{dc}^* = 39$ A.

The iron stator, PM, mechanical and ohmic losses at the rated speed Ω^* are given in Table I; it is worth to point out that the ohmic losses $2RI_{dc}^{*2}$ are prevalent and that the PM losses are about twice the stator iron ones.

The interpolated values of the voltage U_{dc}, calculated by means of the circuit model of Figure 2, are shown in Figure 8. It can be noticed that the voltage drops almost linearly when the current value is below the rated one, while the reduction is more remarkable above such value because of the commutation effects; according to equation (6), a $m \times n = 4 \times 5$ polynomial has been adopted to reproduce the U_{dc} dependence on current and rotor speed.

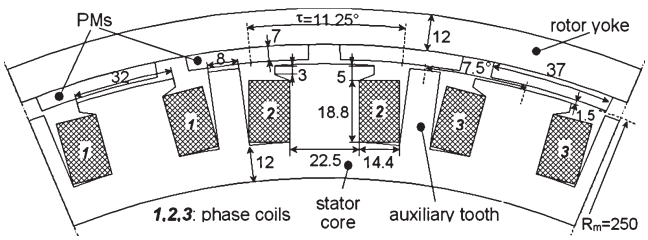

Figure 7. Four poles cross section of the surface-mounted permanent magnet synchronous generator (sizes in mm)

Table I. Iron, PM eddy current and mechanical and winding losses [at rated speed (W)]

p_h^*	p_{ec}^*	p_{ex}^*	P_{fe}	$p_{ec,PM}^*$	P_m	$2RI_{dc}^{*2}$
76.4	36.6	9.9	122.9	227.4	74.9	1704

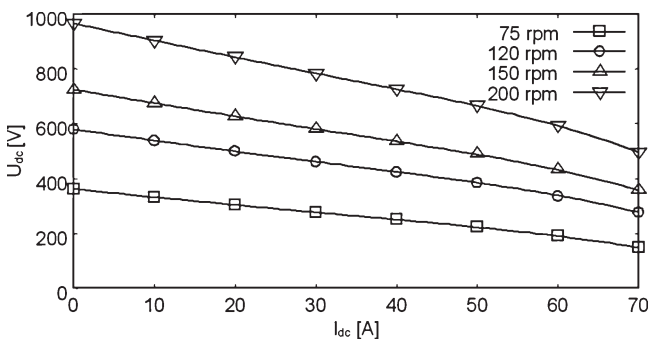

Figure 8. Output voltage U_{dc} interpolation as a function of the load current I_{dc} for different rotor speeds

DOI: 10.1002/we

The power coefficient is defined by the analytical function:[8]

$$C_p(\lambda,\beta) = a_1 e^{\frac{a_5}{\lambda_i(\lambda,\beta)}}\left(\frac{a_2}{\lambda_i(\lambda,\beta)} - a_3\beta - a_4\right) + a_6\lambda$$

with:

$$\lambda_i(\lambda,\beta) = \frac{1}{\dfrac{1}{a_7\beta+\lambda} - \dfrac{a_8}{\beta^3+1}} \tag{29}$$

The values of $a_1, \ldots, a_8$ are given in Table II, which includes other turbine characteristics. By means of equation (29), the interpolating function of the tip-speed ratio is calculated according to equation (22); the curves of Figure 9 confirm the relation between λ and F is not biunique in the range $\lambda < \lambda_M$; anyway, a good correspondence between the initial and the interpolated values is achieved in the stable operation zone ($\lambda \geq \lambda_M$).

Output Characteristics

The circuit model has been used to determine the wind generator characteristics as the wind speed varies, by implementing the proposed control strategy. Both the anemometer presence (Conf.A) and sensorless approach (Conf.B) have been considered.

As shown in Figure 10, there is a good concordance between the results of the two configurations in the whole operating range of the wind speed. In particular, it can be observed that:

- In the range $v \leq v^*$, the turbine operates at $C_{pM,0}$ and the angular speed varies proportionally with the wind speed: in particular, at v^* the rated values of the turbine power ($P_t^* = 22.5$ kW) and of the output power ($P_{dc}^* = 20.46$ kW) are obtained; the corresponding efficiency is $\eta_t^* = P_{dc}^*/P_t^* \approx 0.91$.
- In the range $v^* \leq v \leq v_M = 11.5$ m s^{-1}, the angular speed increases more rapidly than in the previous case because the supplied current is now constant; P_t and P_{dc} are higher than their rated values and attain at v_M their maximum values $P_{t,M} = 35.2$ kW and $P_{dc,M} = 32.36$ kW with an overload $P_{dc,M}/P_{dc}^* = 1.58$ and efficiency

Table II. Turbine characteristics

$\rho = 1.293$ kg m^{-3}	$R_t = 5.1$ m	$C_{pM,0} = 0.48$	$\lambda_M = 8.1$
$v^* = 9.6$ m s^{-1}	$\Omega^* = 15.25$ s^{-1}	$\Omega_M = 23.5$ s^{-1}	$J = 1252$ kg m^2
$a_1 = 0.518$	$a_2 = 116.0$	$a_3 = 0.4$	$a_4 = 5.0$
$a_5 = 21.0$	$a_6 = 0.007$	$a_7 = 0.08$	$a_8 = 0.035$
$t_{fr} = 1.5 \times 10^{-3}$	$t_w = 4 \times 10^{-3}$	$v_{cut,in} = 3.5$ m s^{-1}	$v_{cut,off} = 20$ m s^{-1}

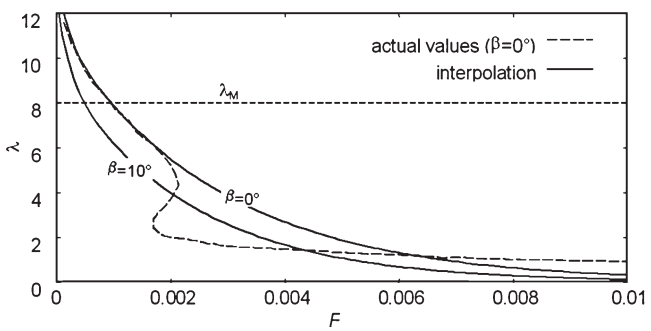

Figure 9. Initial and interpolated values of λ(F), obtained according to equation (22), for two different β values

DOI: 10.1002/we

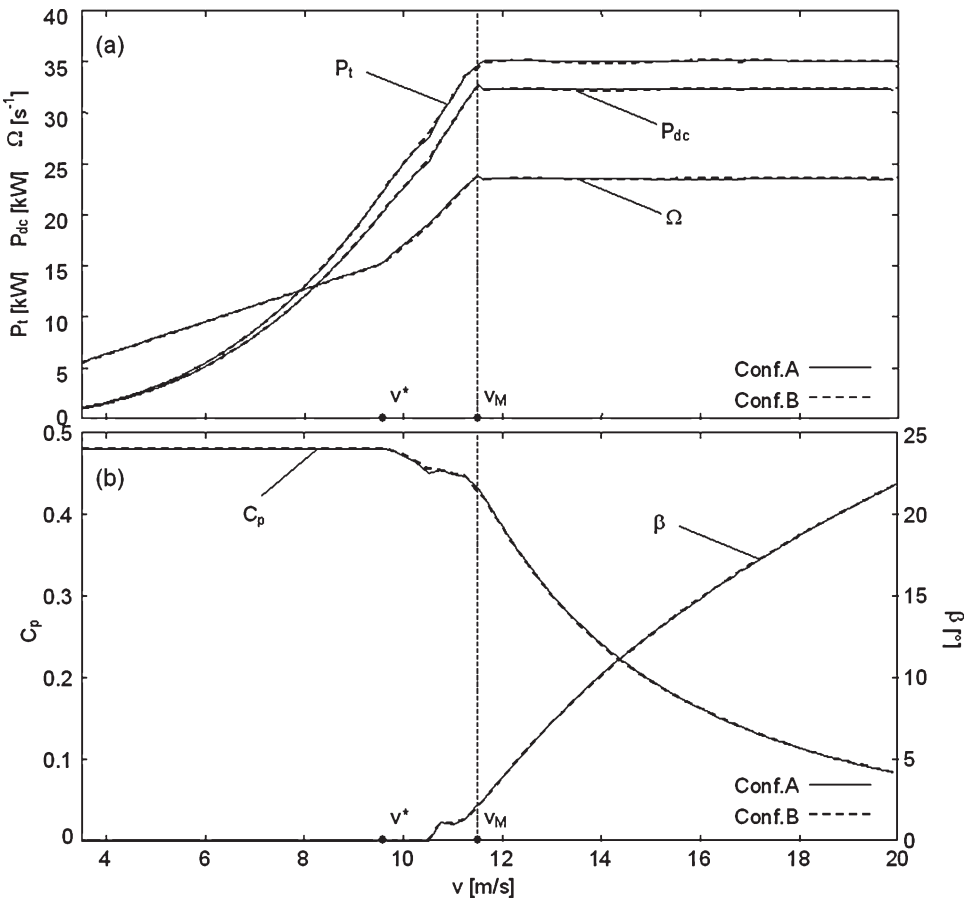

Figure 10. Main operational quantities as functions of the wind speed v for the configuration with and without anemometer: (a) turbine power P_t*, output power* P_{dc} *and rotor speed* Ω*; (b) blade pitch angle* β *and power coefficient* C_p

$\eta_{t,M} = P_{dc,M}/P_{t,M} \approx 0.92$; in this operating range, λ increases slightly reducing the coefficient C_p and preserving stable running conditions.

- In the range $v \geq v_M = 11.5$ m s^{-1}, the pitch angle is regulated to reduce C_p in order to operate at Ω_M, $P_{t,M}$, $P_{dc,M}$, $\eta_{t,M}$.

As mentioned before, the β_r control strategy, adopted for $v \geq v^*$, is based on the determination by equation (17) of the v iso-value curves for different values of $\{\Omega_r,\beta_r\}$ (Figure 11). In this figure, the values of β_r maximizing the corresponding rotor speed reference Ω_r (with the constraint $\Omega_r \leq \Omega_M$) for different wind speed values, are highlighted by dots. The sequence of the corresponding $\{v,\beta_r\}$ pairs provides the maximum allowable output power and can be interpolated by means of an analytical function, implemented in the control system.

Influence of Air Density Variations

In order to test the accuracy and reliability of the control, the influence of variation of the air density variation has been analysed. The air density may heavily affect the turbine performance, as it depends both on the temperature and the altitude of the site (for instance, the available power decreases by about 20% from the sea level up to 2000 m).

DOI: 10.1002/we

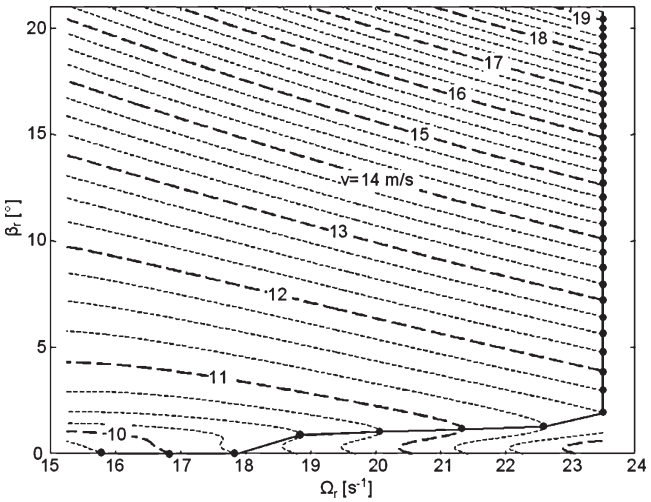

Figure 11. Pitch angle reference β as a function of the rotor speed reference Ω to maximize the output power P_{dc} for different wind speeds v

Table III. Parameters for the current/speed/pitch angle control regulation (c'_k,c''_k expressed by $s^{k-1}A^{-1}$)

$c'_0 = 3.59$	$c'_1 = -0.744$	$c'_2 = 7.7 \times 10^{-2}$	$c'_3 = -3.9 \times 10^{-3}$	$c'_4 = 7.7 \times 10^{-5}$	$c''_0 = 5.4 \times 10^{-2}$	$c''_1 = 2.56 \times 10^{-2}$
$c''_2 = 10^{-5}$	$\tau_R = 20$ s	$\tau_m = 0.01$ s	$\omega_\beta = 10^o$ s^{-1}	$\varepsilon_1 = 0.5$	$\varepsilon_2 = 0.4$	

The mechanical transient from standstill to the steady-state running was simulated with ±10% air density variation with respect to the design value. The current I_{dc} must be controlled to avoid the operation in the unstable zone of the C_p characteristic, the constraints on the maximum allowable current and speed being fulfilled. In particular, in the hypothesis of constant wind speed $v \le v^*$, a lower air density causes the reduction of the current value, operating anyway at $C_{pM,0}$. On the contrary, with higher air density, the current reference cannot exceed I_{dc}^* because of the current limiter: consequently, the rotor speed increases and the power coefficient C_p is lower.

With reference to the relations [equations (20), (27) and (28)] and to Figure 6, the chosen parameters for the control of the current, speed and pitch angle are given in Table III.

The rotor speed profiles resulting from the step application of the rated speed v^* for $k_\Omega = 0.7$, are shown in Figure 12: both the Conf.A and the Conf.B achieve the speed reference value (based on the estimated wind speed in the case of Conf.B), proving the effectiveness of the control system. The dynamical response is, however, quite different, as the sensorless control shows reduced speed overshoots and achieves the steady-state condition more quickly. As regards the steady-state rotor speed, the Conf.A value with 1.1ρ density is higher than the optimum one because of the current limitation; on the contrary, the Conf.B values are different, because of the different estimation of the wind speed evaluated on the basis of the turbine torque according to equation (18). With reference to the output power and efficiency, the data of Table IV show that the behaviour of the configurations is similar, because both the configurations increase the output power proportionally to the air density, the efficiency being practically unchanged.

Influence of Uncertainties in Wind Speed Measurement

In the commercial installations, the wind speed measurement is done by means of anemometers which may have different measurement accuracy and be affected by the turbine interference. This is the cause of uncertainties in the signal of the anemometric sensor, usually between 3 and 20%.[9]

DOI: 10.1002/we

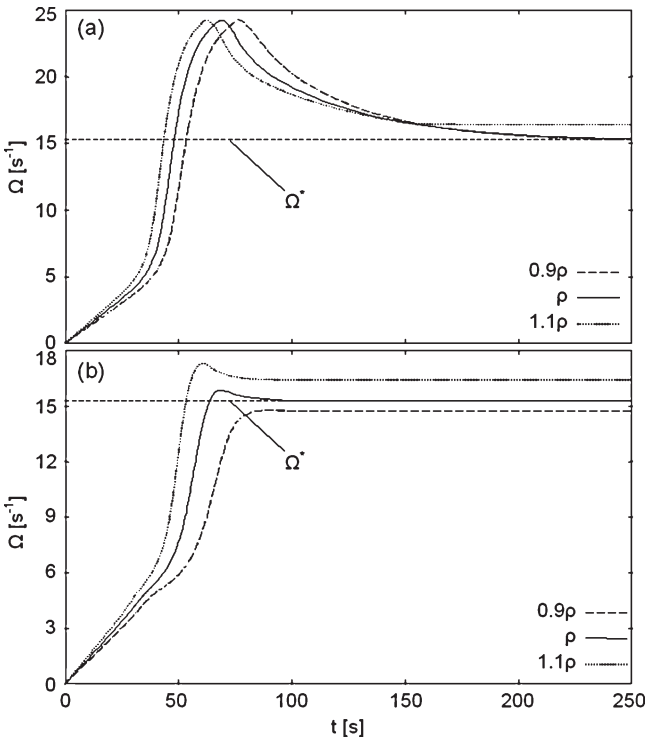

Figure 12. Speed Ω *profiles for different air density values: (a) Conf.A; (b) Conf.B*

Table IV. Output power and efficiency for different air density values

Air density	Conf.A		Conf.B	
	P_{dc} (kW)	η_t (%)	P_{dc} (kW)	η_t (%)
0.9ρ	18.59	0.92	18.39	0.91
ρ	20.46	0.91	20.39	0.91
1.1ρ	22.0	0.91	22.0	0.91

In the following, the variation in the wind generator performance and then the effectiveness of the wind speed control described in the scheme of Figure 5 are evaluated, by assuming a ±10% error with respect to the rated speed value $v^* = 9.6\ \mathrm{m\ s^{-1}}$. The rotor speed transient running from standstill to the steady-state operation is given in Figure 13, with or without the wind speed feedback. Apart from the anemometric error, the profiles with the feedback have lower overshoots and tend to the speed reference more quickly. Anyway, while in the case of speed underestimation, the system correctly attains the rated speed; in the case of wind speed overestimation, the error in steady-state conditions is about +10% with feedback and +27% without feedback. It must be pointed out that, in spite of the speed increase, the output power decreases (2.3 and 6.4%, respectively), because of the reduction of both the power coefficient (to 0.466 and 0.44, respectively) and the delivered current (−16 and −34.7%, respectively). These aspects are quite important in the choice between a sensor-provided and a sensorless system, the second being free from this kind of problems.

DOI: 10.1002/we

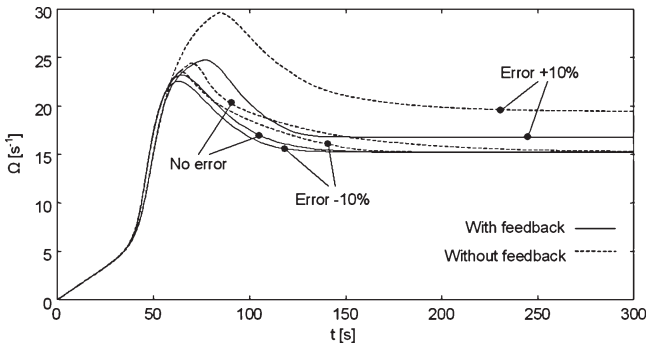

Figure 13. Speed Ω profiles for different anemometer uncertainties with and without wind speed feedback

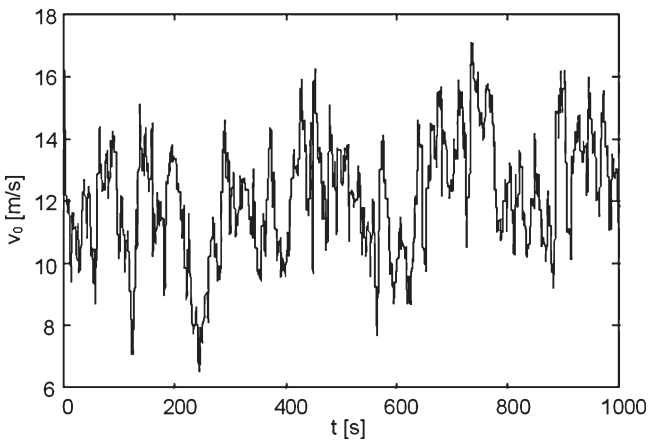

Figure 14. Reference wind speed $v_0(t)$ profile used to test the control algorithms

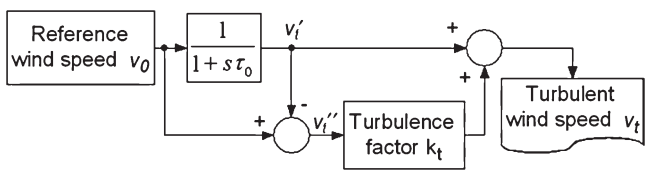

Figure 15. Elaboration of the reference wind speed data v_0 to obtain the turbulent profile v_t

Analysis with Turbulent Wind Conditions

In order to evaluate the effectiveness of the sensorless solution and of the proposed control strategy, it is necessary to verify the progress of the main quantities (output electrical power, angular speed and energy efficiency) following the application of a 'real' wind speed profile, obtained by means of experimental measurements. The reference profile $v_0(t)$, measured in an Italian site for a time interval $t_0 = 1000$ s,[10] is shown in Figure 14. In order to analyse different turbulence conditions, the profile $v_0(t)$ has been elaborated by means of the turbulence factor k_t, which modulates the amplitude of the high-frequency oscillations superimposed to the low-frequency mean value of the speed profile.

The resultant profile $v_t(t)$, used to test the control system, is obtained according to the scheme of Figure 15. The reference signal is filtered through a first-order function ($\tau_0 = 20$ s) to acquire the low-frequency component v_t': by subtracting it from the reference signal, the high-frequency component v_t'' is obtained. The resultant profile is therefore obtained as $v_t = v_t' + k_t \cdot v_t''$: by varying the value of the factor k_t, different turbolence

DOI: 10.1002/we

conditions can be examined and the corresponding energy efficiency can be evaluated. In addition, the starting steady-state speed of the turbine has been assumed to correspond to the wind speed $v = 5$ m s^{-1}, in order to simulate real running conditions.

The output energy W_t and the power coefficient $\langle C_p \rangle$ versus the factor k_t are shown in Figure 16: $\langle C_p \rangle$ is the mean value in the interval t_0 and represents an index to evaluate the deviation from the optimum running conditions. The curves show that the output energy decreases as k_t increases for both the configurations, owing to the delay of the system adjustment to the wind speed variations: this situation is proved by the relevant reduction of $\langle C_p \rangle$, which is 30% lower with respect to the optimum value and more than 20% lower with respect to the value corresponding to the mean speed $\langle v_0 \rangle = 11.9$ m s^{-1} of the reference profile. Actually, simulations show that the deviation (mainly positive) of λ values from λ_M increases with k_t. In addition, the output energy with Conf.B is always higher than the one with Conf.A, and the relative difference increases as k_t increases (up to +7% with $k_t = 1.5$): this is mainly because of the lower promptness of the sensorless system, and the consequent high peaks of the output power increased the delivered energy.

Influence of the Control Parameters of the Pitch Angle Actuator

With reference to both the sensor-provided and sensorless configurations, and to the dual hysteresis band controlling the blade pitch actuator (Figure 6), the influence of the control parameters ε_1 and ε_2 has been evaluated. The analysis is performed by imposing the wind speed profile of Figure 14 (elaborated according to Figure 15), and by applying the turbolence factor $k_t = 1.6$. The calculated quantities are the portion Δt_β of the interval t_0 in which the actuator is on, the output energy W_t and the relative overspeed $\Delta\Omega_M$ defined as:

$$\Delta\Omega_M = \left[\max_{t_0} (\Omega(t)) - \Omega_M \right] \Big/ \Omega_M \tag{30}$$

The comparison of such quantities for both Conf.A and B is given in Table V: the data show that the increasing of the thresholds of the hysteresis controllers does not imply significant variations as regards the maximum overspeed and the overall output energy of the system. On the contrary, it remarkably reduces Δt_β, which is anyway higher in Conf.A because of the better promptness; an adequate promptness is nevertheless necessary to reduce the turbine overspeed mechanical stresses. Vice versa, large threshold values make possible to reduce the stress on the actuator (a quite critical component as regards the system reliability[11]) and then to increase its lifetime.

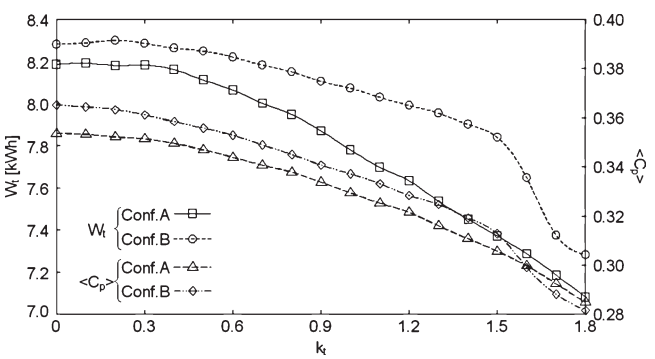

Figure 16. Output energy W_t *and mean power coefficient* $\langle C_p \rangle$ *as functions of the turbulence factor* k_t *for sensor and sensorless control systems*

DOI: 10.1002/we

Table V. Influence of the pitch actuator control parameters on different turbine performances

ε_1	ε_2	$\Delta\Omega_M$ (%)		Δt_β (%)		W_t (kWh)	
		A	B	A	B	A	B
0.10	0.08	6.80	22.43	88.56	76.88	7.290	7.647
0.20	0.16	6.97	22.44	81.23	63.74	7.291	7.647
0.30	0.24	6.97	22.26	74.05	59.10	7.290	7.646
0.40	0.32	7.40	22.22	71.26	53.48	7.281	7.649
0.50	0.40	7.70	21.99	67.30	50.22	7.287	7.648

Conclusions

An integrated circuit model of a wind turbine drive is utilized in the paper to set up advanced control techniques, based on the control of the load current and of the blade pitch angle; the techniques make possible to maximize the wind generator output power in the wind speed operating range, consistently with the electrical, thermal and mechanical design constraints.

In particular, a sensorless algorithm has been developed; such algorithm on the one hand ensures steady-state performances comparable with an anemometer-provided control system (with lower costs for components, installation and maintenance); on the other hand, gives good performance in dynamical conditions. The simulations have indeed confirmed that the sensorless system shows better behaviour with turbulent wind, produces lower stresses on the pitch angle actuator and is obviously free from the problems related to disturbances and measurement uncertainness, which affect the performance of the anemometer-provided systems.

The integration of the circuit model with the control system may be quite useful for quickly evaluating the suitability of a wind energy generation system, permitting to analyse the influence of the mechanical and electrical parameters on the energy efficiency and the system response even with wind turbulence.

References

1. Patel MR. *Wind and Solar Power Systems*. CRC Press: Boca Raton, 1999; 35–69.
2. Grauers A. Synchronous generator and frequency converter in wind turbine applications: system design and efficiency. *Technical Report* N.175 L, Chalmers University of Technology, Göteborg, Sweden, 1994.
3. Andriollo M, Bettanini G, Fasolo A, Martinelli G, Morini A, Tortella A. Sistemi di generazione eolica di piccola potenza. *Atti del 101° Convegno Nazionale AEIT*, Capri, 2006.
4. Andriollo M, Martinelli G, Morini A, Tortella A. Performance assessment of a wind PM generator-rectifier system by an integrated FEM-circuit model. *Proceedings of IEMDC 2007*, Antalya, 2007; 7–12.
5. Fingersh LJ, Johnson KE. Baseline results and future plans for the NREL controls advanced research turbine. *42nd AIAA Aerospace Sciences Meeting and Exhibit*, Reno, 2004; 87–93.
6. Tan K, Islam S. Optimum control strategies for grid-connected wind energy conversion system without mechanical sensors. *IEEE Transactions on Energy Conversion* 2004; **19**: 392–399.
7. Achilles S, Pöller M. Direct drive synchronous machine models for stability assessment of wind farms. *4th International Workshop on Large-scale Integration of Wind Power and Transmission Networks for Offshore Wind Farms*, Billund, 2003; available: http://www.digsilent.de/Consulting/Publications/DirectDrive_Modeling.pdf.
8. Heier S. *Grid Integration of Wind Energy Conversion Systems*. John Wiley & Sons: Chichester, 1998; 34–36.
9. Klug H, Strack M. Technical risks related to wind farm financing. *Proceedings of the AWEA 2002*, Washington, 2002; available: http://www.dewi.de/dewi/fileadmin/pdf/publications/Publikations/klug_techrisks_awea2001.pdf.
10. Romoli P, Pedrazzi C, Alberghino L. Energia dal vento in siti a bassa velocitá ed alta turbolenza: missione impossibile?, 2007. Available: http://www.terom.it.
11. Tavner PJ, Xiang J, Spinato F. Reliability analysis for wind turbines. *Wind Energy* 2006; **10**: 1–18.

DOI: 10.1002/we